RSC Advances

PAPER

View Article Online
View Journal | View Issue

Open Access Article. Published on 30 July 2025. Downloaded on 11/9/2025 12:03:00 PM.
This article is licensed under a Creative Commons Attribution-NonCommercial 3.0 Unported Licence.

Check for updates

Cite this: *RSC Adv.*, 2025, **15**, 27177

Effects of combined UV-tensile aging on structural and electrical properties of high temperature vulcanized silicone rubber in composite insulators

Shiyin Zeng,[a] Wendong Li,[a] Wuji He,[a] Yuelin Liu,[a] Xinyi Yan,[a] Ming Lu,[b] Chao Gao[b] and Guanjun Zhang*[a]

High-temperature vulcanized silicone rubber (HTV-SR) in composite insulators undergoes performance degradation under prolonged ultraviolet (UV) exposure and mechanical stress in plateau environments, posing risks to power grid reliability. To investigate the aging behavior and mechanism of HTV-SR under coupled UV and tensile stress conditions, accelerated aging tests are conducted for 500 hours under constant UV irradiation combined with varying tensile stresses. Surface morphology, structure, mechanical and electrical properties of HTV-SR samples before and after aging are systematically characterized to analyze the synergistic and competitive effects of UV and tensile aging. The results show that UV irradiation induces chain scission and oxidative crosslink, increasing surface crosslink density while deteriorating the mechanical and electrical performance. In contrast, tensile stress alone causes minor structural disturbances due to the inherent elasticity of the material, with limited impact on electrical properties. Under combined aging, tensile stress reduces the effective surface crosslink density and inhibits UV-induced oxidative crosslink. As the tensile ratio increases, molecular chains exhibit more pronounced stress relaxation and filler debonding, further accelerating UV-induced structural and electrical degradation. This study provides theoretical support for the weathering assessment of composite insulators and highlights the importance of maintaining an appropriate crosslink density of HTV-SR to enhance structural and electrical stability in service environments.

Received 3rd June 2025
Accepted 16th July 2025

DOI: 10.1039/d5ra03926f

rsc.li/rsc-advances

1 Introduction

Composite insulators are essential components in high-voltage transmission lines owing to their excellent hydrophobicity, pollution resistance and high mechanical strength. The sheds and sheaths of insulators are made of high-consistency high-temperature vulcanized silicone rubber (HTV-SR), which effectively protects the core rod and enhances insulation performance.[1–3] In service, external mechanical loads are primarily transmitted through the core rod to the sheaths, subjecting the HTV-SR material and its interface to sustained tensile stress.[4] However, long-term exposure to ultraviolet (UV) radiation, tensile stress and corona discharge can significantly degrade the performance of composite insulators, compromising the reliability of transmission lines.[5,6]

To date, a number of studies have investigated the performance of HTV-SR under individual aging factors such as tensile stress or UV irradiation.[7,8] Li *et al.*[9] examined the effects of xenon-lamp UV aging on the surface discharge of SR in dry and humid air, revealing that both degradation and oxidation reactions occurred during UV exposure. Lin *et al.*[10] studied the surface changes of HTV-SR and LSR after UVA irradiation, observing a decrease in surface carbon content and an increase in oxygen content. Additionally, Ma *et al.*[11] analysed the mechanical response of HTV-SR sheds used in high-speed train insulators under continuous wind load, and found that persistent vibration could lead to shed damage or even tearing, increasing the risk of flashover. These studies primarily focus on the aging behaviour under single-stress conditions, which cannot fully reflect actual service environments. In recent years, research into aging mechanisms under combined stress factors has gained increasing attention. For instance, Hu *et al.*[12] investigated the aging behaviour of HTV-SR in cable accessories under thermal and tensile stresses, showing that thermal aging increased crosslink density while tensile stress produced the opposite effect. Nevertheless, the degradation behaviour under the combined influence of UV irradiation and tensile stress remains inadequately addressed.

In the plateau environment, composite insulators are exposed to multiple stressors such as UV irradiation, wind and mechanical vibrations. Vibrations like aeolian motion, galloping, and sub-span oscillation can cause fatigue damage, leading to microcracks on the sheath surface and accelerating

[a]State Key Laboratory of Electrical Insulation and Power Equipment, Xi'an Jiaotong University, Xi'an, Shaanxi 710049, China

[b]State Grid, Henan Electric Power Corporation Electric Power Research Institute, Zhengzhou 450052, China

© 2025 The Author(s). Published by the Royal Society of Chemistry

Open Access Article. Published on 30 July 2025. Downloaded on 11/9/2025 12:03:00 PM.
This article is licensed under a Creative Commons Attribution-NonCommercial 3.0 Unported Licence.

HTV-SR aging.[13] Field observations have shown that aging often initiates at rubber defects near the shed-sheath interface and propagates toward the sheath–core interface.[14] UV irradiation induces chain scission, oxidation and surface chalking, while sustained tensile stress promotes crack growth, resulting in more complex degradation under coupled UV and mechanical stress. Studying the aging behaviour of HTV-SR under UV-tensile coupling is therefore critical for enhancing durability and extending service life. Additionally, varying the tensile ratio during sample preparation enables control of surface crosslink density, allowing investigation into its effect on UV aging.[15,16]

This study investigates the aging behaviour of HTV-SR in composite insulators under the coupled effects of UV irradiation and tensile stress. Constant UV irradiation intensity and varying tensile stress intensities are applied individually and simultaneously over different aging durations. The surface morphology, structural, mechanical and electrical properties are assessed. Based on these results, the aging behaviour of HTV-SR under UV-tensile coupling is summarized, and the underlying mechanism are further discussed.

2 Experimental details

2.1 Sample preparation

The silicone rubber used in this study is a high-consistency rubber, commonly referred to as HTV-SR in engineering practice. The HTV-SR samples used in this study are provided by Xiangyang State Grid Composite Insulator Co., Ltd. The material is composed of 100 parts vinyl-terminated poly(-methylvinylsiloxane), 33 parts hydrophilic fumed silica (8 nm, specific surface area: 195 m^2 g^{-1}), 130 parts aluminium hydroxide (ATH) powder (1.7 μm), 6 parts hydroxyl-terminated silicone oil and 5 parts Fe_2O_3 (0.8 μm) (all parts by weight). The components are blended using a 50 Hz kneader and subjected to brief thermal treatment at 150 °C for 10 min to promote homogeneous dispersion. The blended rubber is then filtered and cooled to room temperature. For vulcanization, approximately 1 part of 2,5-dimethyl-2,5-di(*tert*-butylperoxy) hexane is added below 70 °C, followed by heating to 170 °C to complete crosslinking.[17] The cured HTV-SR is cut into block specimens measuring 6 × 10 × 0.2 cm^3.

2.2 Test apparatus and test method

To investigate the aging behaviour of HTV-SR under coupled UV-tensile conditions, an accelerated aging platform is established. Compared to other light sources, xenon lamps offer a spectral distribution that closely resembles natural sunlight, making them suitable for simulating long-term UV exposure in outdoor environments. Fig. 1 illustrates the basic structure of the UV xenon lamp aging chamber. The system employs optical filters to effectively eliminate infrared wavelengths, thereby ensuring a stable UV irradiation environment. To ensure adequate UV exposure while minimizing thermal radiation effects, the distance between the samples and the lamp is set to 30 cm based on the standard ASTM G155. The xenon light source provides a theoretical UV irradiance of approximately 3.3 mW cm^{-2} (290–400 nm) at the sample surface, as provided by the equipment manufacturer. However, the actual irradiance decreases with increasing distance between the sample and the light source. As shown in Fig. 2, samples are stretched to tensile ratios of 20%, 40% and 60% using a custom-built tensile fixture. The tensile ratio is defined as the relative increase in length compared to the initial sample length.[18] While held in the stretched state, the specimens are exposed to constant-intensity UV irradiation inside the aging chamber. Continuous ventilation is maintained throughout the process to simulate a realistic UV-mechanical coupled aging environment encountered during service.

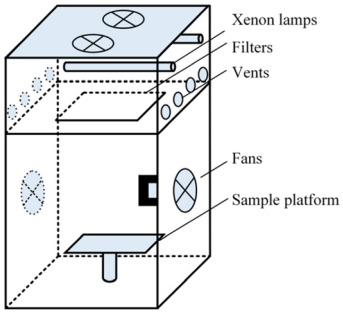

Fig. 1 Schematic diagram of the UV xenon lamp aging chamber.

Accordingly, five experimental groups are designed, as summarized in Table 1. Two groups are subjected to single-factor aging conditions: one to UV exposure without mechanical strain (denoted as "U"), and the other to 60% tensile strain without UV exposure (denoted as "L3"). Unaged samples served as the control group. All aging tests are conducted for a duration of 500 hours. Due to the variation in tensile stress, the degree of oxidative crosslinking per unit surface area of HTV-SR may differ. Therefore, the "UL1" to "UL3" groups are designed under constant UV intensity with varying tensile ratios. This setup not only enables investigation of the role of tensile strain in the coupled aging process but also provides insight into how different crosslink structures affect the UV aging behaviour of the HTV-SR material.

2.3 Characterization

2.3.1 Surface morphology. Three-dimensional surface topography and roughness of the samples are measured using a laser confocal microscope (Keyence VK-X150, Japan). Surface

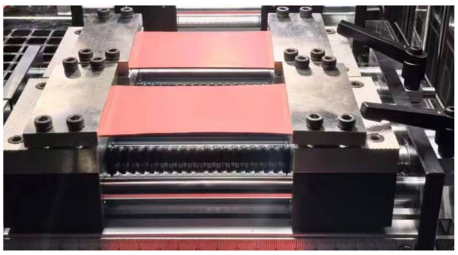

Fig. 2 Photo of the tensile fixture for SR samples.

 © 2025 The Author(s). Published by the Royal Society of Chemistry

Open Access Article. Published on 30 July 2025. Downloaded on 11/9/2025 12:03:00 PM.
This article is licensed under a Creative Commons Attribution-NonCommercial 3.0 Unported Licence.

Table 1 Multi-factor aging test program considering temperature cycling

Group	UV irradiation power	Stretching ratio	Aging time (h)
U	On	—	500
L3	Off	60%	
UL1	On	20%	
UL2	On	40%	
UL3	On	60%	

microstructural details are further examined by scanning electron microscopy (SEM, VE-9800S, Keyence, Osaka, Japan).

2.3.2 Structural properties. Chemical bonding structures are characterized by Fourier-transform infrared spectroscopy (FTIR, Nicolet IN10 + IZ10, Thermo Fisher Scientific, Waltham, MA, USA).[19] X-ray photoelectron spectroscopy (XPS) is performed using a Thermo Scientific K-Alpha system, while crystalline structure analysis is conducted *via* X-ray diffraction (XRD, Bruker D8 Advance, Germany). Crosslink density is quantified by the equilibrium swelling method.[20] Small rubber specimens are immersed in toluene for 7 days until fully swollen, and measurements are taken twice to obtain the average value.

2.3.3 Mechanical properties. The hardness of specimens is measured by a Shore durometer (LX-A). Tensile properties are evaluated using a computer-controlled universal testing machine (5 kN) with type IV dumbbell-shaped specimens in accordance with GB/T 528-2009. Each sample is tested 3 times and the average value is calculated

2.3.4 Electrical Properties. Surface flashover voltage is measured under ambient conditions using classical circular electrodes with a radius of 10 mm and spacing of 4 mm. A DC voltage is applied at a ramp rate of approximately 1 kV s^{-1} until flashover occurred.[21] The ambient temperature and relative humidity during testing are maintained at 25 °C and 35%, respectively. Each sample is tested 12 times and the average is calculated. Dielectric properties are characterized using a broadband dielectric spectrometer (Novocontrol Concept 80, Montabaur, Germany) over the frequency range of 0.1 Hz to 10 000 Hz at room temperature. Copper electrodes are employed for the measurements, with the upper electrode having a diameter of 22 mm and the lower electrode 38 mm. A test voltage of 1 V is applied. Surface resistivity is measured at room temperature using a high-resistance electrometer (6517B, Keithley, USA) equipped with a three-electrode fixture (Model 8009). Each sample is measured 8 times and the mean value is recorded.

3 Results and discussion

3.1 Surface morphology

Fig. 3 presents the changes in the three-dimensional surface morphology of the HTV-SR material before and after aging. The unaged sample exhibits a relatively smooth surface, whereas the UV-aged sample (U) shows noticeable surface particulates. In contrast, the sample subjected only to tensile aging (L3) shows a small number of tiny pores. This suggests that, under single-factor aging, UV exposure has a more pronounced impact on surface structure than tensile stress, likely due to UV-induced photo-oxidation. In comparison, sample UL3 exhibits significantly increased surface roughness along with more severe surface defects, indicating that the combined effect of UV irradiation and tensile stress accelerates surface deterioration.

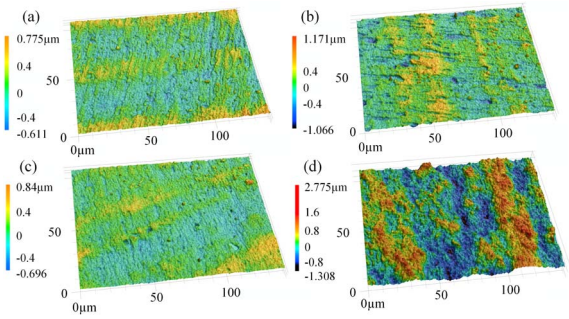

Fig. 3 3D surface morphology of HTV-SR samples under different aging conditions: (a) unaged sample; (b) sample U; (c) sample L3; (d) sample UL3.

To further investigate surface morphological changes, Fig. 4 presents SEM images of HTV-SR samples subjected to different aging conditions. Compared with the relatively smooth and intact surface of the unaged sample, sample U shows slight deposition of particulate matter, while sample L3 exhibits the presence of microcracks. Compared with single-factor aging, the combined effects of UV irradiation and tensile stress promote the formation of surface grooves and the expansion of holes. As the tensile ratio increases, the surface defect area progressively enlarges, likely due to the synergistic acceleration

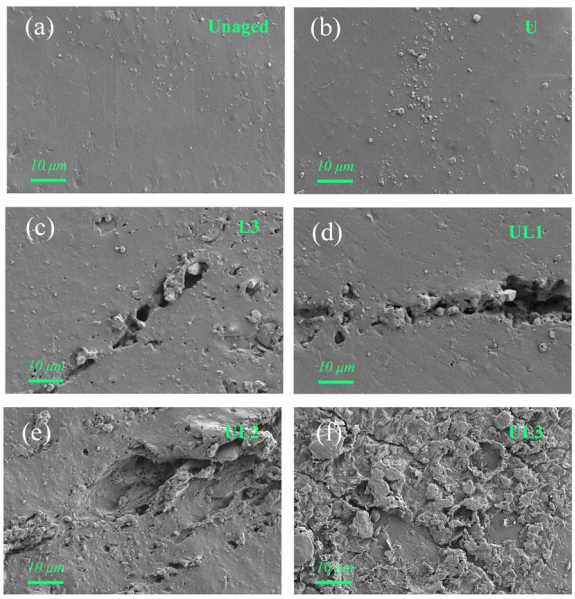

Fig. 4 SEM photos of HTV-SR samples under different aging conditions: (a) unaged sample; (b) sample U; (c) sample L3; (d) sample UL1; (e) sample UL2; (f) sample UL3.

Open Access Article. Published on 30 July 2025. Downloaded on 11/9/2025 12:03:00 PM.
This article is licensed under a Creative Commons Attribution-NonCommercial 3.0 Unported Licence.

of crack initiation and propagation under UV-tensile coupling effect. Interestingly, in sample UL3, no clear cracks are observed. Instead, a flocculent layer appears to cover the surface, which is presumed to consist of low-molecular-weight (LMW) products and precipitated inorganic fillers. This layer likely masks the underlying cracks and indicates that the material has entered a more deepened stage of degradation.

3.2 Structural and mechanical properties

The internal crosslink density of HTV-SR is further investigated and analysed. The volume fraction of the swollen polymer (V_2) is first calculated using the following equation:[22]

$$V_2 = \frac{m_1 b/\rho_1}{m_1 b/\rho_1 + (m_2 - m_1)\rho_t} \quad (1)$$

where m_1 is the initial sample mass, m_2 is the mass after full swelling, b is the mass fraction of siloxane in HTV-SR (as provided by the manufacturer), ρ_1 and ρ_t are the densities of HTV-SR and toluene, respectively ($\rho_t = 0.866$ g cm^{-3}). Subsequently, the crosslink density of HTV-SR is calculated using the following equation:

$$D_C = \frac{-[\ln(1 - v_2) + v_2 + \alpha v_2^2]}{2\rho_t V_t (v_2^{1/3} - v_2/2)} \quad (2)$$

where α is the polymer–solvent interaction parameter between HTV-SR and toluene ($\alpha = 0.545$), and V_t is the molar volume of toluene ($V_t = 106.7$ cm^3 mol^{-1}).

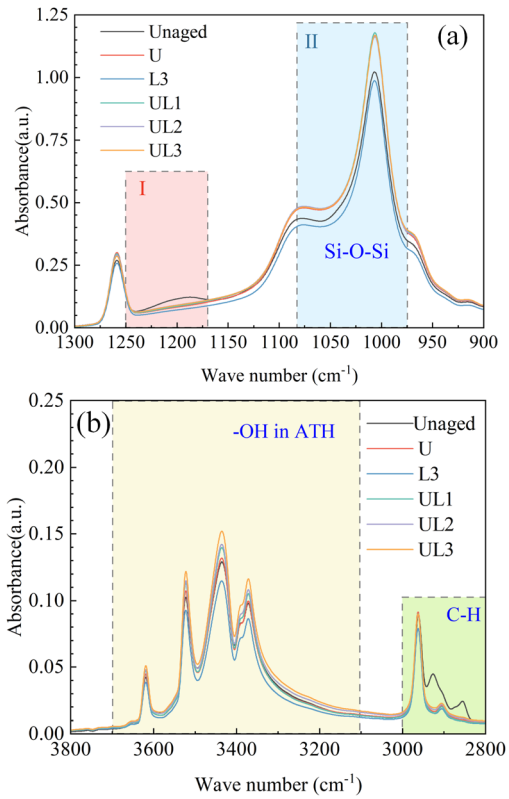

Fig. 5 FTIR spectra of HTV-SR under different aging conditions: (a) 1300–900 cm^{-1}; (b) 3800–2800 cm^{-1}.

To evaluate the molecular structural changes in HTV-SR before and after aging, Fig. 5 presents the FTIR spectra of samples subjected to different aging conditions. Two characteristic regions can be identified within the 1300–900 cm^{-1} range. Region I correspond to amorphous silica, exhibiting a broad shoulder around 1220 cm^{-1}. Region II is associated with long-chain or branched Si–O–Si networks characterized by bond angles less than 144°, along with stretched Si–O bonds on the pore surfaces.[23] In Region I, the absorption peak is significantly weakened or even disappears after UV or tensile aging. This may be attributed to the disruption of the filler-matrix interface or aggregation of SiO_2 particles during aging, which reduces their surface activity and makes the corresponding absorption signals less detectable. In Region II, the intensity of the Si–O–Si characteristic peak increases under UV-only and combined UV-tensile aging, but slightly decreases in the tensile-only aging. It suggests that UV irradiation promotes the formation of Si–O–Si linkages *via* oxidative crosslink. Moreover, by examining the –OH groups in ATH at 3700–3100 cm^{-1}, an increase in the –OH peak is observed in samples subjected to UV-involved aging, suggesting the surface exposure of ATH fillers. In contrast, the –OH peak decreases in samples aged under tensile stress alone. Additionally, analysis of the C–H stretching vibrations reveals a significant reduction in peak intensity after aging. This reduction is primarily attributed to UV-induced main chain scission, which degrade side groups. In the case of tensile-only aged samples, the overall reduction in infrared peak intensity may result from chain alignment or local relaxation, thereby weakening the absorption response.

The crosslink density of aged HTV-SR samples is presented in Fig. 6. Sample U exhibits a higher crosslink density than sample L3, indicating that UV irradiation promotes the formation of oxidative crosslinking networks on the material surface. In contrast, the reduction in crosslink density observed in sample L3, which underwent tensile aging alone, may be attributed to the Mullins effect—a stress-induced phenomenon in rubber materials where cyclic or sustained loading leads to irreversible microstructural rearrangement.[24] This includes filler-matrix debonding and polymer chain slippage, which loosens the physical network. Under combined UV-tensile

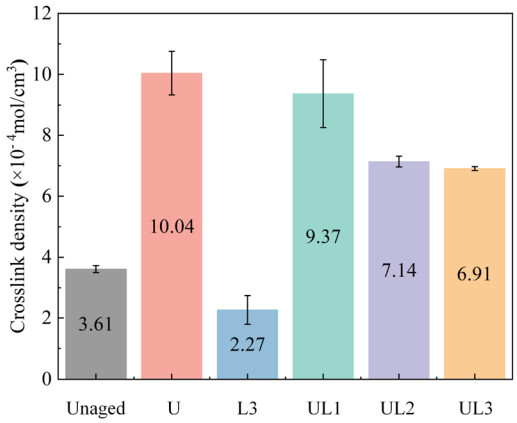

Fig. 6 Crosslink density of HTV-SR under different aging conditions.

 © 2025 The Author(s). Published by the Royal Society of Chemistry

Open Access Article. Published on 30 July 2025. Downloaded on 11/9/2025 12:03:00 PM.
This article is licensed under a Creative Commons Attribution-NonCommercial 3.0 Unported Licence.

aging, the crosslink density decreases progressively with increasing tensile strain. This trend suggests that sustained mechanical stress not only promotes physical relaxation of the network but may also hinder UV-induced chemical crosslink, thereby reducing the overall crosslink density of HTV-SR. The insignificant difference in crosslink density between UL2 and UL3 may be attributed to the compensating effect of UV-induced oxidative crosslink, which offsets the additional network disruption under higher tensile strain.

To further investigate changes in Si–O structural units, XPS is employed to analyse the HTV-SR samples. Silicon in the material primarily exists in the forms of $Si(-O)_2$, $Si(-O)_3$ and $Si(-O)_4$, with corresponding binding energies of 102.1 eV, 102.8 eV and 103.4 eV, respectively.[9] The Si 2p spectra are deconvoluted to quantify the relative content of each chemical state, as shown in Fig. 7 and Table 2.

In the unaged HTV-SR sample, $Si(-O)_2$ is primarily attributed to the Si–O–Si backbone of the silicone rubber, while $Si(-O)_4$ is originally introduced through the SiO_2 filler.[25] The presence of highly oxidized Si, namely $Si(-O)_3$ and $Si(-O)_4$, is generally considered indicative of increased crosslinking and oxidation levels.[26] The results show that the content of highly-oxidated Si atoms increases after aging compared to the unaged sample, which is consistent with the crosslink density. As for the single-factor aging groups, sample U exhibits a notably higher $Si(-O)_4$ content, reaching 11.8%, suggesting that UV irradiation promotes more uniform surface oxidation, thereby increasing

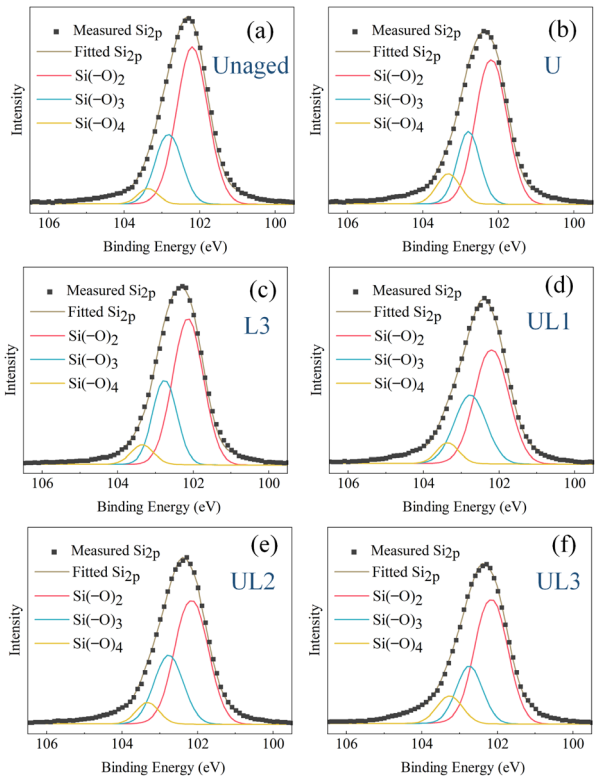

Fig. 7 XPS results of HTV-SR under different aging conditions: (a) unaged sample; (b) sample U; (c) sample L3; (d) sample UL1; (e) sample UL2; (f) sample UL3.

Table 2 Relative compositions of Si–O structures of samples under different aging conditions

Sample	$Si(-O)_2$	$Si(-O)_3$	$Si(-O)_4$	Highly oxidized Si ($Si(-O)_3$+$Si(-O)_4$)
Unaged	64.9%	28.6%	6.5%	35.1%
U	58.8%	29.4%	11.8%	41.2%
L3	58.8%	33.5%	7.7%	41.2%
UL1	56.2%	33.7%	10.1%	43.8%
UL2	57.8%	32.4%	9.8%	42.2%
UL3	59.5%	27.4%	13.1%	40.5%

the formation of $Si(-O)_4$ structures. In contrast, sample L3 shows a slight increase in $Si(-O)_3$, which may be attributed to molecular chain reorientation or local segment migration during stretching, making the flexible PDMS chains more exposed. This surface change by XPS contrasts with the reduced bulk crosslink density due to the Mullins effect, highlighting the difference between surface and bulk under mechanical aging. In the combined aging groups (UL1–UL3), the proportion of highly-oxidated Si atoms gradually decreases from 43.8% to 40.5%, possibly due to the tensile stress reducing the crosslink density and oxidative activity per unit surface area, thereby limiting the accumulation of highly oxidated structures. Interestingly, sample UL3 exhibits the highest $Si(-O)_4$ content at 13.1%, which may be associated with accelerated surface degradation and SiO_2 filler precipitation caused by the synergistic aging effect.[27]

To investigate differences in surface filler composition under various aging conditions, XRD results of HTV-SR samples are presented in Fig. 8. The PDMS backbone exhibits an amorphous structure with long-range disorder and short-range order, typically characterized by a broad diffuse peak around $2\theta = 11°$.[28] Previous studies have shown that unaged HTV-SR without ATH fillers displays a distinct amorphous silica diffraction peak near $2\theta = 22°$. However, upon incorporating a high proportion of ATH, its sharp crystalline peaks dominate the XRD pattern, overshadowing the characteristic "hump" associated with fumed silica.[29] In the UV-aged sample, the XRD spectrum is primarily composed of diffraction peaks from ATH and iron oxide (mainly hematite), while no clear amorphous features are observed. The disappearance of the PDMS-related amorphous peak may result from radical-induced degradation of the polymer backbone under UV exposure. In contrast, the tensile-only aged sample retains more of the original structural features, suggesting that such degradation is not activated under mechanical stress alone. To further compare filler evolution across different aging groups, the relative content of ATH and iron oxide are analysed. Compared to the unaged sample, the ATH content in sample U decreases to 95.5%, while it remains nearly unchanged in sample L3, indicating that UV exposure possibly promoted the precipitation of silica and Fe_2O_3 particles. Besides, it is inferred that prolonged UV exposure may induce photothermal effects that locally elevate surface temperature, promoting the partial dehydration of ATH particles to form Al_2O_3.[30,31] Under combined aging, the ATH content

Open Access Article. Published on 30 July 2025. Downloaded on 11/9/2025 12:03:00 PM.
This article is licensed under a Creative Commons Attribution-NonCommercial 3.0 Unported Licence.

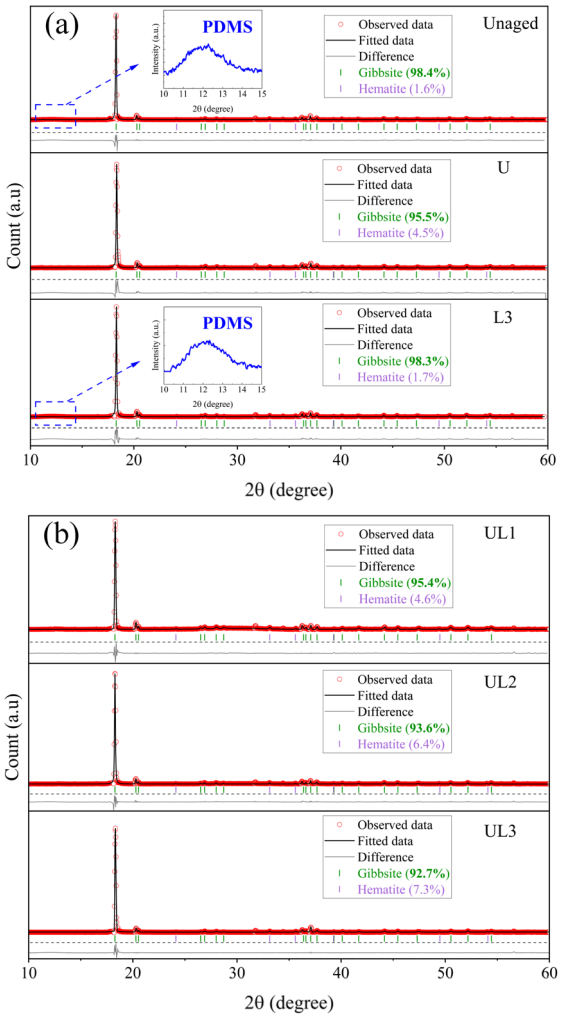

Fig. 8 XRD results of HTV-SR specimens under different aging conditions: (a) unaged sample, sample U and L3; (b) sample UL1, UL2 and UL3.

further declined with increasing tensile stress, reaching 92.7%, confirming that UV-tensile coupling intensifies surface degradation, leading to accelerated filler precipitation.

To explore the correlation between microstructural changes and macroscopic mechanical performance, Fig. 9 presents the variation in elongation at break and hardness of HTV-SR samples before and after aging. Compared to the unaged sample, the average elongation at break in both the UV-aged and tensile-aged groups shows no significant change. In the tensile-aged sample, the slight increase in elongation may be attributed to the Mullins effect, wherein repeated or sustained loading leads to stress-softening and chain alignment, allowing the material to deform more before failure. Under combined UV-tensile aging, elongation at break progressively decreases with increasing tensile ratio, implying that backbone scission and crosslink network degradation significantly reduce the material's ductility.[32] Meanwhile, the hardness of aged samples shows a moderate increase, likely due to the formation of a stiffer surface layer from UV-induced crosslinking. This dual

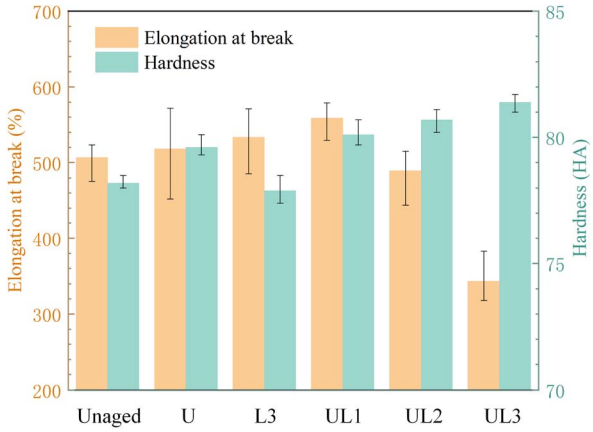

Fig. 9 Elongation at break and hardness of HTV-SR under different aging conditions.

mechanism leads to a decrease in bulk crosslink density and elongation at break, while the surface hardness shows an increasing trend. These observations highlight the inhomogeneous nature of aging in HTV-SR, where UV-induced surface stiffening and mechanically induced internal relaxation coexist and compete.

3.3 Electrical properties

To evaluate changes in insulation performance, the surface resistivity of HTV-SR samples before and after aging is measured, as shown in Fig. 10. The results indicate that sample L3 shows negligible change compared to the unaged sample, while the sample U exhibits a significant 74.0% decrease in surface resistivity. Under combined aging, surface resistivity progressively decreases with increasing tensile ratio, further confirming the synergistic degradation effect of UV exposure and tensile stress. This suggests that tensile loading exacerbates UV-induced microstructural changes, such as filler precipitation or defect propagation, ultimately leading to a more pronounced decline in insulation performance. This result aligns with the Fe_2O_3 content variations observed in the XRD patterns (Fig. 8). As a semiconductive oxide, the increased surface presence of Fe_2O_3 facilitates charge transport, thereby contributing to the reduced surface resistivity in UV-aged HTV-SR. In contrast, tensile aging alone induces minimal change in Fe_2O_3 content, consistent with the stable resistivity observed in sample L3.

To further assess the surface insulation performance of HTV-SR, DC flashover tests are conducted to evaluate its surface discharge resistance. The experimental data are fitted using the Weibull distribution function and the fitting results are presented in Fig. 11.

$$F(V_s) = 1 - \exp\left(-\left(\frac{V_s}{\alpha}\right)^{\beta}\right) \tag{3}$$

where V_s is the flashover voltage, $F(V_s)$ represents the cumulative probability of flashover, α is the scale parameter (corresponding to a 63.2% probability of failure) and β is the shape parameter.

 © 2025 The Author(s). Published by the Royal Society of Chemistry

Open Access Article. Published on 30 July 2025. Downloaded on 11/9/2025 12:03:00 PM.
This article is licensed under a Creative Commons Attribution-NonCommercial 3.0 Unported Licence.

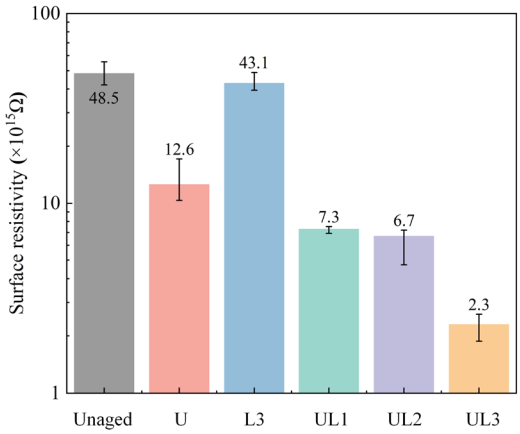

Fig. 10 Surface resistivity of the HTV-SR samples under different aging conditions.

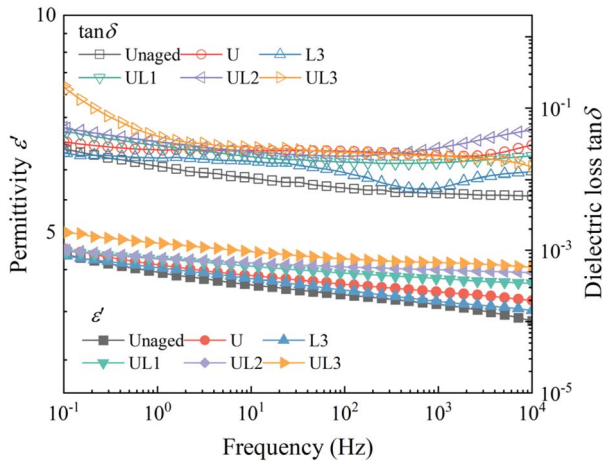

Fig. 12 Dielectric spectra of HTV-SR samples under different aging conditions.

The results indicate that, compared with the unaged sample, sample L3 shows a relatively small decrease in the scale parameter α, whereas sample U exhibits a more pronounced reduction. This suggests that UV exposure has a greater impact on surface insulation performance, likely due to UV-induced oxidative crosslinking. For the UV-tensile aged samples, α shows a slight decreasing trend with increasing tensile ratio, but the overall variation remains limited. Unlike surface resistivity, the tensile ratio appears to have a less significant effect on surface flashover voltage. This may be attributed to the fact that, under UV-dominated aging, tensile stress did not induce extensive surface cracking or continuous conductive pathways and the surface remained relatively intact, thus maintaining a comparatively high flashover voltage.[9]

To further analyse the dielectric properties and the evolution of polarization and loss during aging, the real part of the dielectric constant (ε') and the dielectric loss tangent (tan δ) for both unaged and aged HTV-SR samples are presented in Fig. 12. The results show that ε' increases across the entire frequency range after aging, with the smallest change observed in the tensile-aged sample (L3) and the largest in the UV-tensile aged sample (UL3). Similarly, tan δ also increases for all aged samples over the full frequency domain, with the most significant rise occurring in the combined aging group. These findings further confirm the synergistic effect of UV exposure and tensile stress in accelerating the degradation of the material's dielectric performance.

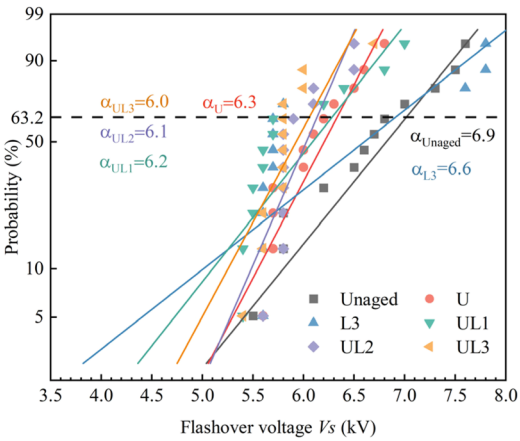

Fig. 11 DC flashover probability of HTV-SR samples under different aging conditions.

To enable a more detailed quantitative analysis of the dielectric spectra, the Havriliak–Negami (H–N) dielectric relaxation model is employed to resolve the multiple relaxation processes.

$$\varepsilon^* = \varepsilon_\infty + \sum_{i=1}^{3} \frac{\Delta\varepsilon_i}{[1+(iw\tau_i)^{m_i}]^{n_i}} + \frac{\sigma_{DC}}{i\varepsilon_0 w} \tag{4}$$

In this model, ε^* denotes the complex permittivity, while ε_∞ represents the permittivity at the optical frequency limit. $\Delta\varepsilon_i$ and τ_i correspond to the strength and characteristic relaxation time of three relaxation processes, respectively. m_i and n_i describe the degree of dispersion for each relaxation. σ_{DC} denotes the DC conductivity and ω is the angular frequency.[33]

Fig. 13 shows the H–N model fitting of the imaginary permittivity (ε'') for aged HTV-SR samples, revealing good agreement across all groups. The dielectric response primarily comprises DC conductivity, Maxwell–Wagner–Sillars (MWS) relaxation, and β-relaxation. Since some relaxation peaks lie outside the measurement range (10^{-1}–10^4 Hz), only those within the range and with intensities $>10^{-2}$ are listed in Table 3. The DC conductivity remains largely unchanged after aging, indicating no significant deterioration in conductivity under the applied UV and tensile conditions. While MWS relaxation remains stable in single-stress aged samples, it increases in the combined-stress aged group, especially in sample UL3. This enhancement likely results from interfacial defects (*e.g.*, voids, agglomerates, microcracks) that impair compatibility between fillers and matrix, intensifying interfacial polarization.[34] Moreover, both UV-only and combined aging samples exhibit stronger β-relaxation, suggesting UV-induced degradation of the PDMS backbone and the generation of LMW fragments.[35]

Open Access Article. Published on 30 July 2025. Downloaded on 11/9/2025 12:03:00 PM.
This article is licensed under a Creative Commons Attribution-NonCommercial 3.0 Unported Licence.

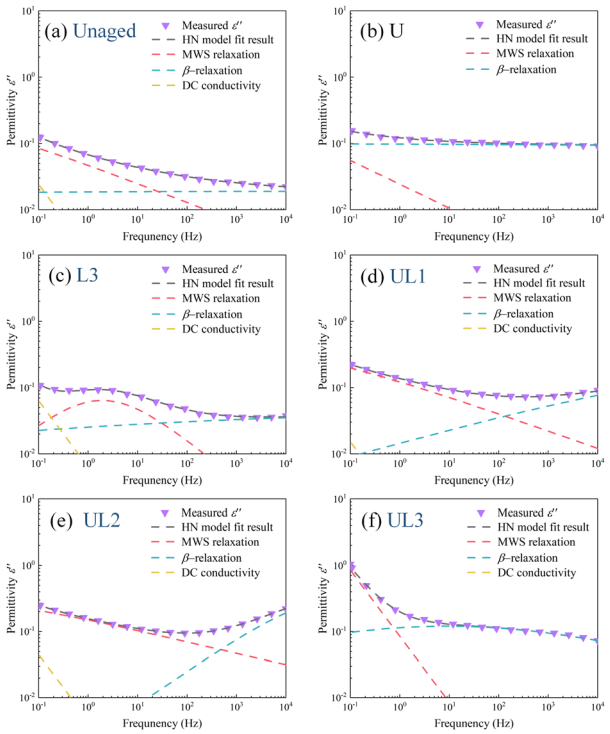

Fig. 13 XPS results of HTV-SR under different aging conditions: (a) unaged sample; (b) sample U; (c) sample L3; (d) sample UL1; (e) sample UL2; (f) sample UL3.

Table 3 Maximum intensity of relaxations of different HTV-SR samples in the frequency range

Group	Unaged	U	L3	UL1	UL2	UL3
DC conductivity	0.02	—	0.06	0.01	0.05	—
MWS-relaxation	0.06	0.07	0.07	0.19	0.21	0.85
β-relaxation	0.02	0.09	0.03	0.08	0.19	0.13

These fragments enhance dipolar polarization, contributing to the observed increase in β-relaxation intensity.

3.4 Discussions

Based on the analysis of crosslink density and XPS results, a competitive effect between UV and tensile aging is proposed. As illustrated in Fig. 14, under UV aging, high-energy UV irradiation can induce polymer backbone scission and oxidative crosslink, leading to the production of LMWs and filler precipitation, resulting in surface microstructural defects (see Fig. 14a).[36] Under tensile stress alone, the high elasticity of HTV-SR allows molecular chains to gradually recover their original configuration upon stress release, causing only slight disturbance to the crosslinking network, which are insufficient to trigger significant changes in electrical properties.[12] This degradation is further associated with the Mullins effect, which causes irreversible softening and crosslink density reduction under high strain. In contrast, during combined UV-tensile aging, although UV-induced oxidative crosslink initially increases crosslink density (see Fig. 14b and c), it also reduces

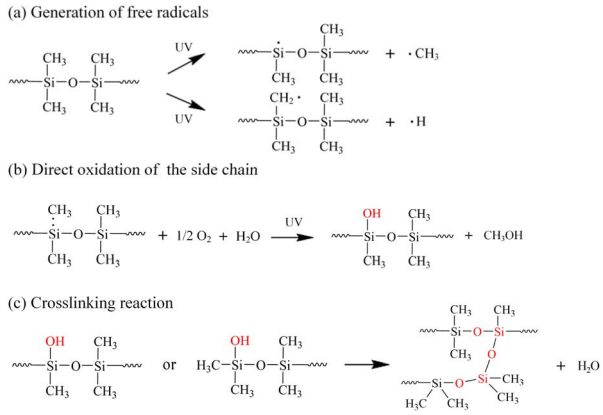

Fig. 14 Reactions of HTV-SR during UV aging: (a) genaration of free radicals; (b) direct oxidation of the side chain; (c) crosslinking reaction.

the material's elasticity, making tensile-induced deformation less reversible. Under high tensile ratios, sustained mechanical stress promotes the scission of PDMS chains, which subsequently reduces the local crosslink network density and may suppress or even disrupt UV-induced crosslink. This ultimately results in a decrease in both overall crosslink density and the proportion of highly-oxidated Si atoms, reflecting a competitive interaction between the two aging mechanisms.

The synergistic effects between UV and tensile aging are reflected in multiple aspects of the degradation process, including surface morphology changes, filler decomposition and migration, as well as the deterioration of mechanical and electrical properties. As illustrated in Fig. 15, under tensile stress, PDMS chains undergo orientation and rearrangement, which promotes debonding, migration and even exposure of embedded inorganic fillers (such as SiO_2 or ATH). This phenomenon becomes more pronounced when the crosslink network is severely damaged. Such filler displacement weakens the interfacial bonding between the matrix and the fillers, leading to particle deposition,

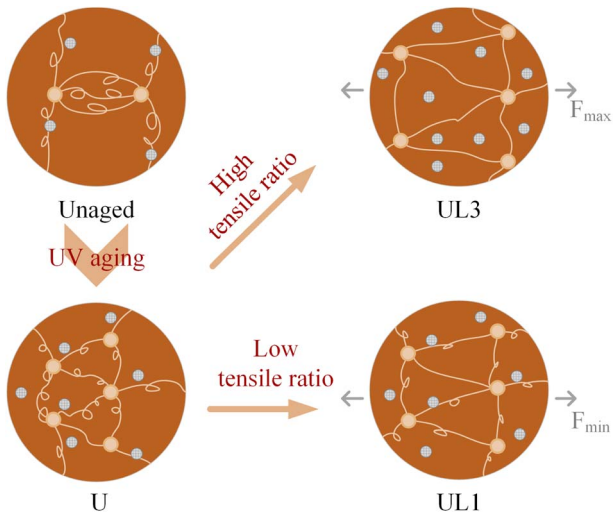

Fig. 15 States of molecular chains of HTV-SR and fillers under UV and tensile effects.

 © 2025 The Author(s). Published by the Royal Society of Chemistry

Open Access Article. Published on 30 July 2025. Downloaded on 11/9/2025 12:03:00 PM.
This article is licensed under a Creative Commons Attribution-NonCommercial 3.0 Unported Licence.

increased surface roughness and deteriorated electrical performance. With increasing tensile ratios, PDMS chains exhibit more pronounced stress relaxation and filler debonding behaviour. As a result, UV-induced degradation of surface structure, electrical insulation and mechanical strength becomes more prominent in the coupled aging condition, demonstrating a typical synergistic acceleration effect.

In addition, this study systematically evaluated the performance evolution of HTV-SR during UV aging by applying different tensile ratios to modify the surface crosslink network structure. The results demonstrate that tensile stress induces chain orientation and structural relaxation, leading to a reduction in crosslink density, which in turn compromises the stability of the surface network and the material's resistance to aging. A moderately high crosslink density contributes to maintaining the integrity of the three-dimensional network, suppressing chain mobility and microstructural degradation, thereby enhancing resistance to UV-induced oxidation, crack formation and overall performance deterioration. Furthermore, a stable crosslinked structure improves interfacial bonding between the polymer matrix and inorganic fillers, reducing the likelihood of filler migration or precipitation. In summary, maintaining a high crosslink density is crucial for improving the UV aging resistance and electrical stability of HTV-SR materials.

4 Conclusions

This study presents a comprehensive investigation into the effects of UV exposure and tensile stress on HTV-SR used in composite insulators, simulating plateau-like conditions. The aging behaviour of surface morphology, structure, mechanical and electrical properties is systematically analysed.

(1) A UV-tensile coupled aging approach is developed to reveal the synergistic and competitive effects between UV irradiation and tensile stress. By varying the tensile ratio, the influence of crosslink density on UV aging performance is explored.

(2) UV irradiation induces polymer chain scission and oxidative crosslink, increasing crosslink density and generating surface degradation products. In contrast, tensile aging alone causes only minor structural changes due to the material's elasticity.

(3) In combined aging, competition between UV-induced crosslink and tensile-induced relaxation leads to reduced crosslink density and decreased highly-oxidated Si atoms. Meanwhile, synergistic effects are evident in the accelerated degradation of surface morphology, mechanical strength and insulation performance. Maintaining relatively high crosslink density is found to be critical for improving UV resistance and electrical stability.

Data availability

The data supporting this article have been included as part of the manuscript and it will be made available upon a reasonable request.

Author contributions

Shiyin Zeng: conceptualization, methodology, formal analysis and investigation, writing – original draft. Wendong Li: validation, resources, data curation. Wuji He: resources, data curation. Yuelin Liu: conceptualization, methodology. Xinyi Yan: formal analysis and investigation. Ming Lu: visualization. Chao gao: resources, data curation. Guanjun Zhang: supervision, writing – review & editing, funding acquisition, project administration.

Conflicts of interest

There are no conflicts to declare.

Acknowledgements

The authors kindly acknowledge the financial support of the Major Special Science and Technology Project of State Grid Henan Electric Power Company (grant no. 521702240006) and Xiangyang Guowang Composite Insulators Co., Ltd, Hubei, China.

References

1 M. X. Zhu, J. Y. Xue, Y. H. Wei, G. C. Li and G. J. Zhang, Review of interface tailoring techniques and applications to improve insulation performance, *High Voltage*, 2022, **7**(1), 12–31.
2 G. N. Wu, Y. H. Fan, Y. J. Guo, S. Xiao, Y. Liu, G. Q. Gao and X. Q. Zhang, Aging mechanisms and evaluation methods of silicone rubber Insulator sheds: A review, *IEEE Trans. Dielectr. Electr. Insul.*, 2024, **31**(2), 965–979.
3 J. Y. Guo, Y. M. Wang, Y. W. Wang, F. H. Yin, T. Q. Liu, F. Masoud and Y. Lin, Characteristic properties of High Consistency Rubber and Liquid Silicone Rubber, in *Proceedings of IEEE Conference on Electrical Insulation and Dielectric Phenomena*, 2018, pp. 21–24.
4 F. L. Zhang, Transferring mechanism of mechanical of mechanical property of press-tight joint interface for composite insulator and determination of assembling parameter, *Power Syst. Technol.*, 2001, **1**, 47–53.
5 M. Akbar, R. Ullah and S. Alam, Aging of silicone rubber-based composite insulators under multi-stressed conditions: an overview, *Mater. Res. Express*, 2019, **6**(10), 102003.
6 N. C. Mavrikakis, P. N. Mikropoulos and K. Siderakis, Evaluation of field-ageing effects on insulating materials of composite suspension insulators, *IEEE Trans. Dielectr. Electr. Insul.*, 2017, **24**(1), 490–498.
7 G. J. Zhang, L. Zhao, R. D. Zhou, W. W. Shen and X. D. Liang, Review on aging characterization and evaluation of silicon rubber composite insulator, *High Voltage Appar.*, 2016, **52**, 1–15.
8 K. Sit, A. K. Pradhan, B. Chatterjee and S. Dalai, A review on characteristics and assessment techniques of high voltage

Open Access Article. Published on 30 July 2025. Downloaded on 11/9/2025 12:03:00 PM. This article is licensed under a Creative Commons Attribution-NonCommercial 3.0 Unported Licence.

silicone rubber insulator, *IEEE Trans. Dielectr. Electr. Insul.*, 2022, **29**(5), 1889–1903.

9 Z. Li, L. Sun, S. C. Liu, J. H. Li, Z. Q. Ma, L. L. Cai, Z. G. Wang, J. Liu and S. T. Li, Influence mechanisms of ultraviolet irradiation aging on DC surface discharge properties of silicone rubber in dry and humid air, *Appl. Surf. Sci.*, 2024, **678**, 161107.

10 Y. Lin, F. H. Yin, Y. H. Liu and L. M. Wang, Influence of vulcanization factors on UV-A resistance of silicone rubber for outdoor insulators, *IEEE Trans. Dielectr. Electr. Insul.*, 2020, **27**(1), 296–304.

11 J. Q. Ma, W. W. Wang, X. F. Wang, J. H. Geng, K. Chen and Y. Y. Bao, Analysis of sheath edge corrosion of EMU roof epoxy resin insulator in 57 m/s high speed wind tunnel, *High Voltage Apparatus*, 2020, **46**(7), 2496–2503.

12 H. Hu, Z. D. Jia and X. L. Wang, Aging mechanism of silicone rubber under thermal-tensile coupling effect, *IEEE Trans. Dielectr. Electr. Insul.*, 2022, **29**, 185–192.

13 X. D. Liang, Y. F. Gao, J. F. Wang and S. H. Li, Rapid development of silicone rubber composite insulator in China, *High Voltage Eng.*, 2016, **42**, 2888–2896.

14 Y. N. Peng, W. D. Li, S. Y. Zeng, Y. C. Zhang, Y. Deng and B. Peng, Reproduction and analysis of decay-like aging development induced by interfacial discharge in composite insulators, *IEEE Trans. Dielectr. Electr. Insul.*, 2023, **30**(4), 1858–1867.

15 S. Ansorge, F. Schmuck and K. O. Papailiou, Impact of different fillers and filler treatments on the erosion suppression mechanism of silicone rubber for use as outdoor insulation material, *IEEE Trans. Dielectr. Electr. Insul.*, 2015, **22**(2), 979–988.

16 S. Ansorge, F. Schmuck and K. O. Papailiou, Improved silicone rubbers for the use as housing material in composite insulators, *IEEE Trans. Dielectr. Electr. Insul.*, 2012, **19**(1), 209–217.

17 S. Y. Zeng, W. D. Li, Y. N. Peng, Y. C. Zhang and G. J. Zhang, Mechanism of accelerated deterioration of high-temperature vulcanized silicone rubber under multi-factor aging tests considering temperature cycling, *Polymers*, 2023, **15**(15), 3210.

18 Y. Liu and X. Wang, Research on property variation of silicone rubber and EPDM rubber under interfacial multi-stresses, *IEEE Trans. Dielectr. Electr. Insul.*, 2019, **26**(6), 2027–2035.

19 A. Cristy, Chapter 3 Theory of infrared spectroscopy, *Compr. Anal. Chem.*, 2001, **35**, 19–40.

20 S. Gehrke, in *Synthesis, equilibrium swelling, kinetics, permeability and applications of environmentally responsive gels*, Springer, 2005, 1, pp. 81–144.

21 S. Y. Zeng, W. D. Li, X. Zhao, Y. N. Peng, Y. L. Liu, X. Y. Yan and G. J. Zhang, Degradation of HTV silicone rubber in composite insulators under UVB-corona coupling effect in simulated plateau environments, *Polym. Degrad. Stab.*, 2025, **238**, 11354.

22 W. Chassé, M. Lang, J. U. Sommer and K. Saalwächter, Crosslink density estimation of PDMS networks with precise consideration of networks defects, *Macromolecules*, 2012, **45**(2), 899–912.

23 Z. D. Jia, C. Xu, R. Y. Guan, X. L. Wang and Y. Deng, Simulation of the chalking of silicone rubber based on tetramethylammonium-hydroxide-catalyzed scission reaction, *Polym. Degrad. Stab.*, 2023, **208**, 110251.

24 J. Diani, B. Fayolle and P. Gilormini, A review on the Mullins effect, *Eur. Polym. J.*, 2009, **45**(3), 601–612.

25 W. L. Bao, X. D. Liang, Y. Y. Liu, Y. F. Gao and J. F. Wang, Effects of AC and DC corona on the surface properties of silicone rubber: Characterization by contact angle measurements and XPS high resolution scan, *IEEE Trans. Dielectr. Electr. Insul.*, 2017, **24**(5), 2911–2919.

26 C. Xu, N. P. Yan, C. J. Yang, X. L. Wang and Z. D. Jia, Effects of platinum catalyst on the dielectric properties of addition cure silicone rubber/SiO2 nanocomposites, *IEEE Trans. Dielectr. Electr. Insul.*, 2021, **28**(1), 142–149.

27 S. Y. Zeng, X. Zhao, W. D. Li, Y. N. Peng, Y. L. Liu, X. Y. Yan and G. J. Zhang, Performance comparison and lifespan assessment of naturally and artificially chalked silicone rubber for composite insulators, *Polym. Degrad. Stab.*, 2025, **232**, 111139.

28 J. Lancastre, N. Fernandes, F. Margaça, I. Salvado, L. Ferreira, A. Falcão and M. Casimiro, Study of PDMS conformation in PDMS-based hybrid materials prepared by gamma irradiation, *Radiat. Phys. Chem.*, 2012, **81**(9), 1336–1340.

29 G. Nallathambi, T. Ramachandran, V. Rajendran and R. Palanivelu, Effect of silica nanoparticles and BTCA on physical properties of cotton fabrics, *Mater. Res.*, 2011, **14**, 552–559.

30 J. P. Habas, J. M. Arrouy and F. Perrot, Effects of electric partial discharges on the rheological and chemical properties of polymers used in HV composite insulators after railway service, *IEEE Trans. Dielectr. Electr. Insul.*, 2009, **16**(5), 1444–1454.

31 T. Liang, Z. Zhang, X. Ma, Y. Xiang, H. Huang and X. Jiang, Characteristics of powdered layer on silicone rubber surface, *J. Mater. Res. Technol.*, 2021, **14**, 36–46.

32 J. Kang, K. Choi, W. Jo and S. Hsu, Structure-property relationships of polyimides: a molecular simulation approach, *Polymer*, 1998, **39**(26), 7079–7087.

33 Y. Zhang, W. Li, C. Wang, J. Li, P. Sun, J. Deng and G. Zhang, Eco-friendly thermoplastic alternatives to epoxy resin for support insulators, *IEEE Trans. Dielectr. Electr. Insul.*, 2023, **30**, 518–527.

34 H. Hu, Z. Jia, X. Wang, R. Guan and W. Fan, Simin LuoAnalysis of conductance and interfacial polarisation behaviours of silicone rubber based on frequency domain spectroscopy, *High Voltage*, 2024, **9**(1), 56–65.

35 W. Chao, Y. Gao, X. Liang, S. Gubanski, Q. Wang, W. Bao and S. Li, Manifestation of interactions of nano-silica in silicone rubber investigated by low-frequency dielectric spectroscopy and mechanical tests, *Polymers*, 2019, **11**, 717.

36 R. Y. Wang, Z. F. Dou, Z. H. Liu, N. Li and X. R. Liu, Research on ultraviolet degradation behavior and aging mechanisms of fluorosilicone rubber in simulated tropical marine atmospheric environment, *Polym. Degrad. Stab.*, 2025, **233**, 111153.

 © 2025 The Author(s). Published by the Royal Society of Chemistry